Editors' Suggestion

Orbital State Manipulation of a Diamond Nitrogen-Vacancy Center Using a Mechanical Resonator

H. Y. Chen, E. R. MacQuarrie, and G. D. Fuchs*
Cornell University, Ithaca, New York 14853, USA

(Received 18 January 2018; published 17 April 2018)

We study the resonant optical transitions of a single nitrogen-vacancy (NV) center that is coherently dressed by a strong mechanical drive. Using a gigahertz-frequency diamond mechanical resonator that is strain coupled to a NV center's orbital states, we demonstrate coherent Raman sidebands out to the ninth order and orbital-phonon interactions that mix the two excited-state orbital branches. These interactions are spectroscopically revealed through a multiphonon Rabi splitting of the orbital branches which scales as a function of resonator driving amplitude and is successfully reproduced in a quantum model. Finally, we discuss the application of mechanical driving to engineering NV-center orbital states.

DOI: 10.1103/PhysRevLett.120.167401

Quantum control of diamond NV centers has enabled scientific accomplishments ranging from fundamental tests of quantum mechanics [1] to precision metrology [2–4] and quantum information science [5]. Full state control in the NV-center spin manifold has been realized through several techniques developed over the last decade, including magnetic [6–8], optical [9–11], and mechanical [12–17] methods. In contrast, manipulation of a NV center within its excited-state orbital manifold is both less explored and more difficult because direct transitions between excited-state orbital branches through a magnetic dipole interaction are forbidden. However, the intrinsic coupling between NV-center orbital states and lattice strain [18,19] offers a promising approach to coherently engineering NV-center orbital states, potentially enabling quantum information transfer between NV centers, phonon thermometry [20], cooling of a mechanical resonator [21], and decoherence protection of orbital states.

These applications have drawn growing interest in NV-center orbital-strain interactions. For example, wavelength and polarization tuning of NV-center optical transitions [22] have been demonstrated using quasistatic lattice strain modulation within a diamond cantilever. Recently, Raman sideband transitions from a strain-modulated NV center have been observed using a surface acoustic wave device to manipulate the spin using Λ-system dynamics near the sideband [23,24]. These pioneering experiments motivate additional research aimed at understanding the essential tools and interactions that enable strain-based coherent orbital control of NV centers. Of particular interest are NV-resonator systems that operate in the resolved-sideband limit in which gigahertz-frequency strain oscillations can be treated as coherent phonons.

In this Letter, we directly engineer the NV-center excited orbital manifold using coherent phonons generated by a gigahertz-frequency mechanical resonator. In addition to observing up to nine coherent Raman sideband orders, we demonstrate phonon-induced Rabi splitting of the NV-center excited orbital states as a function of resonator driving amplitude and show a signature of multiphonon orbital transitions. Finally, we show that such orbital-phonon interactions apply to the full spin-orbital fine structure of the NV-center excited states.

For our experiment, we fabricated a diamond high-overtone bulk-mode acoustic resonator (HBAR) device that consists of a zinc oxide piezoelectric transducer patterned on the surface of a type IIa diamond substrate, purchased from Element Six [Fig. 1(a)]. We designed the thickness of the piezoelectric layer to accommodate a mechanical resonance centered around $\omega_m/2\pi \simeq 1.3$ GHz. On driving the transducer, a longitudinal strain wave enters the acoustic cavity formed by the parallel [100] diamond surfaces. On the opposite diamond face, we also patterned a microwave antenna for conventional magnetic resonance manipulation of the NV-center spin.

The orbital-singlet, spin-triplet ground states of a NV center $|^3A_2\rangle$ are coupled to the first excited-state manifold $|^3E\rangle$ through an optical transition with a zero-phonon line (ZPL) at 637.2 nm. The $|^3E\rangle$ manifold consists of six levels, $|E_{x,y}\rangle$, $|E_{1,2}\rangle$, and $|A_{1,2}\rangle$. Strain distortions of the NV centers couple strongly to the orbital components of $|^3E\rangle$, both globally shifting all the states and splitting them into two orbital branches [Fig. 1(b)] [25]. Strain of the NV center can originate either from static stress that is intrinsic to the crystal or from external stress modulation. Using group theory analysis, we can factor the strain coupling into three terms according to the symmetry of the deformation [26,27]: A_1, E_1, and E_2. A_1 induces a global shift of the excited state energies of the NV center with respect to the ground states since it retains the C_{3v} symmetry of the

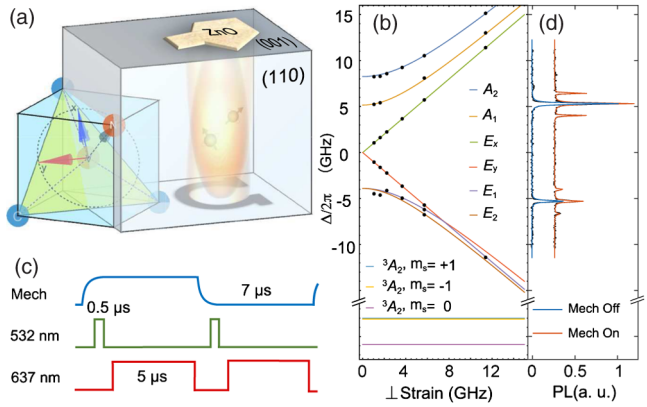

FIG. 1. (a) Device geometry and structure of a NV center inside a diamond unit cell (blue cube). A uniaxial stress wave is generated through the top zinc oxide transducer. Microwave antenna on the bottom provides magnetic manipulation of a NV-center spin. (b) NV-center excited-state and ground-state level diagrams as a function of transverse strain. Experimental data (black dots) show excellent agreement with Ref. [19]. (c) PLE sequence for phonon-dressed state measurement. (d) PLE spectrum of a single NV center with 10.6 GHz static strain splitting between E_x and E_y states (blue curve). A 32 μW drive to the transducer excites phonon sideband transitions (red curve).

defect. In contrast, E_1 and E_2 lower the symmetry and thus split and mix the E states. In the basis of $|E_x\rangle$ and $|E_y\rangle$ states, the strain Hamiltonian takes the Jahn-Teller form [28]

$$H = V_{A_1} I + V_{E_1}\sigma_z + V_{E_2}\sigma_x, \tag{1}$$

where V_i is the deformation potential of i-type symmetry, I is the identity matrix, and σ_z, σ_x are Pauli matrices.

Although static local strain sets the equilibrium orbital state energies of a particular NV center, coherent phonon perturbations can further modify the orbital structure into phonon-dressed states, $|E_{x,y}, n\rangle$, where n is the coherent phonon number. In particular, the uniaxial stress wave generated within the HBAR device excites A_1 and E_1 phonon modes [29]. Therefore, the orbital state strain Hamiltonian becomes

$$H = (V_{A_1} + \mathcal{A}\cos\omega_m t)I + (V_{E_1} + \mathcal{E}_1\cos\omega_m t)\sigma_z + V_{E_2}\sigma_x, \tag{2}$$

where $\mathcal{A}(\mathcal{E}_1)$ characterizes the strength of the $A_1(E_1)$ components of the phonons excited at the mechanical resonator frequency ω_m. We retain V_{A_1}, V_{E_1}, and V_{E_2} from Eq. (1) to parametrize the static strain induced energy shifting and splitting of the NV center.

Experimentally, we probe the orbital-phonon-dressed states through photoluminescence excitation (PLE) spectroscopy at zero applied magnetic field. The HBAR device is first cooled to 10 K in a helium-flow microscopy cryostat. Using our home-built scanning confocal microscope, we locate and isolate a single NV center. To perform PLE, we sweep the frequency of a 637.2 nm tunable laser across the resonant optical transitions and monitor the incoherent phonon sideband fluorescence above 670 nm with a single photon detector. We use a scanning Fabry-Perot cavity to quantify the tunable laser frequency. Figure 1(c) shows the experimental sequence that we use to study phonon-dressed optical transitions. First, we turn on the strain modulation for a period of 7 μs. We include a 2 μs delay to allow the resonator to ring up (quality factor $\simeq$1500). Within that initial delay, we use a 532 nm laser to optically pump the charge of the NV center into the NV^- state and the spin into the $m_s = 0$ state. After ring up, we turn on the tunable laser and collect photons for the remaining 5 μs. As a control, we repeat the cycle except without driving the mechanical resonator.

Because the initialized, unexcited state of the NV center is $|^3A_2, m_s = 0\rangle$, resonant optical excitations connect $|^3A_2, m_s = 0\rangle$ to $|E_x\rangle$ and $|E_y\rangle$ in the excited state. Thus, we initially restrict our study to pure orbital-strain interactions in the spin-zero-state manifold. Taking into account the photon driving field from the tunable laser, the Hamiltonian of the driven system after applying the rotating wave approximation can be written as

$$\begin{aligned} H(m_s = 0) = {} & (-\hbar\Delta + \mathcal{A}\cos\omega_m t)(|x\rangle\langle x| + |y\rangle\langle y|) \\ & + (V_{E_1} + \mathcal{E}_1\cos\omega_m t)(|x\rangle\langle x| - |y\rangle\langle y|) \\ & + V_{E_2}(|x\rangle\langle y| + |y\rangle\langle x|) \\ & + \frac{\hbar}{2}\Omega(|g\rangle\langle x| + |x\rangle\langle g| + |g\rangle\langle y| + |y\rangle\langle g|), \end{aligned} \tag{3}$$

where $|x\rangle$, $|y\rangle$, and $|g\rangle$ are simplified notation for $|E_x\rangle$, $|E_y\rangle$, and the ground state $|^3A_2, m_s = 0\rangle$. Here, $\Delta = \omega_l - \omega_0 - V_{A_1}/\hbar$ is the laser detuning, ω_0 is the unperturbed NV-center transition frequency, and Ω is the optical Rabi frequency. Because of the inhomogeneity of the stress within the sample, we observed NV centers with $\{|E_x\rangle, |E_y\rangle\}$ state splitting ranging from 2 to 30 GHz [Fig. 1(b)]. Figure 1(d) shows PLE spectra taken from a NV center with a static orbital splitting of 10.6 GHz, both with and without (32 μW to the transducer) mechanical driving. We immediately see that mechanical driving introduces resolved sidebands to each of the two optical transitions in the PLE spectrum. We also note that because NV centers positioned near an antinode of the resonator are deep within the diamond bulk (>30 μm below the diamond surface for the NV centers studied in this paper), charge fluctuations are smaller than for near-surface NV centers [30]. Thus, we obtain typical PLE linewidths of 100 MHz for optical power of 830 nW. In this work, we select NV centers with orbital strain splittings of 10.6, 3.2, and 2.1 GHz and study their PLE spectra as we vary the

driving power to the transducer from 0 to 10 mW. Based on the variation of the PLE linewidth, we estimate that sample heating is less than 5 K.

First, we study a NV center (labeled NV1) with a static strain splitting of 10.6 GHz [Fig. 2(a)], which is many times larger than $\omega_m/2\pi = 1.3844$ GHz. In the presence of mechanical driving, coherent Raman sideband transitions appear at $\Delta = \pm n\omega_m$ with respect to the undriven optical resonance frequencies due to photon-phonon coupling. Specifically, it arises from A_1 modulation of the E states through the $\mathcal{A}\cos\omega_m t$ term in Eq. (3) [Fig. 2(b)]. This effect is from sideband-resolved frequency modulation, which can arise in both classical and quantum resonances [17,31–34].

As the mechanical driving strength increases, up to $n = 9$ sideband orders emerge at a driving power of 10 mW [Fig. 2(b)]. We expect that the amplitude of each sideband transition varies according to a Bessel function form $J_n^2(\mathcal{A}/\hbar\omega_m)$, which can be derived from either the rotating wave approximation [35] or Floquet theory [36]. Because of laser-power broadening, however, the sideband order peaks are described by $\{[s_0 J_n^2(\mathcal{A}/\hbar\omega_m)]/[1 + s_0 J_n^2(\mathcal{A}/\hbar\omega_m)]\}$ [Fig. 2(d)], where $s_0 = 2\Omega^2/\Gamma^2$ is the saturation parameter and Γ is the linewidth of a NV-center optical transition [37].

A second prominent feature in the dressed spectral evolution of NV1 is the repulsive frequency shift of the two orbital branches, including sidebands, as a function of mechanical driving amplitude: $|E_y\rangle(|E_x\rangle)$ branches are subject to red (blue) shifts in frequency [Fig. 2(b)]. This is caused by E_1-modulation-induced Rabi splitting of the E states in the presence of nonzero V_{E_2}, which becomes clear by applying a polaron transformation [38–40] to the orbital state strain Hamiltonian. In the displaced oscillator orbital basis, Eq. (2) becomes [29]

$$H' = \begin{pmatrix} -\hbar\omega_m + \Delta_x + \mathcal{A}\cos\omega_m t & -\mathcal{E}_1 \sin 2\theta \sum_n J_n(2\frac{\mathcal{E}_1}{\hbar\omega_m}\cos 2\theta) e^{-in\omega_m t} \\ -\mathcal{E}_1 \sin 2\theta \sum_n J_n(2\frac{\mathcal{E}_1}{\hbar\omega_m}\cos 2\theta) e^{in\omega_m t} & -\Delta_x + \mathcal{A}\cos\omega_m t \end{pmatrix}, \quad (4)$$

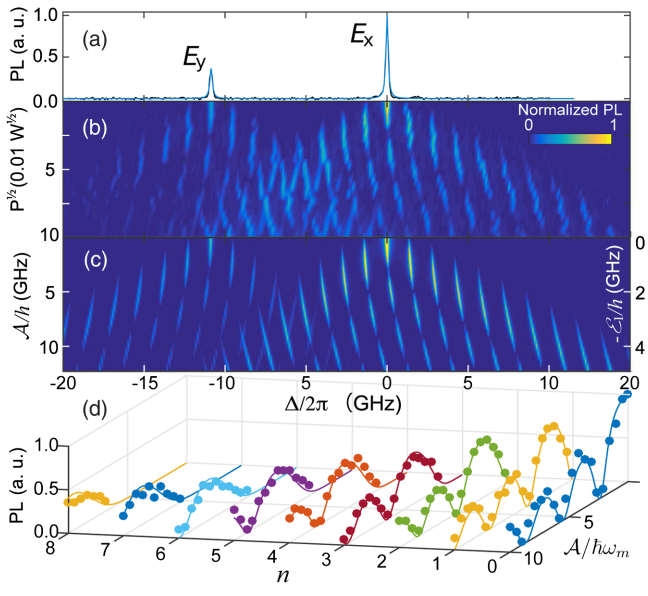

FIG. 2. (a) PLE spectrum of NV1 with $\{|E_x\rangle, |E_y\rangle\}$ state splitting of 10.6 GHz in the absence of mechanical driving. (b) Phonon-dressed state PLE measurement with $\omega_m/2\pi = 1.3844$ GHz. The mechanical driving amplitude is proportional to square root of the power applied to the transducer, $P^{1/2}$. Sideband transitions and level repulsion are evident in between E states. (c) Reconstruction of experimental data through quantum master equation simulation. (d) E_x sideband transition ($n = 0$ to 8) photoluminescence peak amplitude (solid dots) plotted against theoretical prediction (solid line), which is not a fit to the data.

where θ is the mixing angle of the static strain deformation potential defined by $\tan 2\theta = V_{E_2}/V_{E_1}$. Also, $2\Delta_x = 2\sqrt{V_{E_1}^2 + V_{E_2}^2}$ is the static strain splitting of E states, and J_n is the Bessel function of the first kind of order n. The off-diagonal terms in Eq. (4) characterize the $(n+1)$-phonon coupling of orbital states from E_1 modulation, which give rise to multiphonon driven orbital transitions [29] when the resonance condition $(n+1)\hbar\omega_m = 2\Delta_x$ is satisfied.

To further study this effect, we select a different NV center (NV2) with a comparably small static E state splitting, 3.2 GHz, which we can bring into a 2-phonon resonance by driving with a mechanical mode frequency of $\omega_m/2\pi = 1.6$ GHz. Figure 3 shows the resulting spectra as a function of $\mathcal{E}_1$ amplitude. As $\mathcal{E}_1$ increases, the individual orbital levels first split linearly, while the splitting starts to decrease at a higher $\mathcal{E}_1$ amplitude. This phonon Rabi splitting is well described by the $n = 1$ coupling term in Eq. (4) $\mathcal{E}_1 \sin 2\theta J_1\{2[\mathcal{E}_1/(\hbar\omega_m)]\cos 2\theta\}$ [outlined by the white dashed lines in Fig. 3(b)], with a small deviation caused by the contribution of off-resonant phonon interactions of other orders, $n + 1 \neq 2$, indicating that the resonant 2-phonon process dominates the dressed orbital states under these conditions.

To quantitatively model the general case of phonon-dressed orbital states, we implement a quantum master equation simulation [29]. We adjust $\mathcal{A}$ and $\mathcal{E}_1$ as free parameters by hand to match the calculated spectra to the

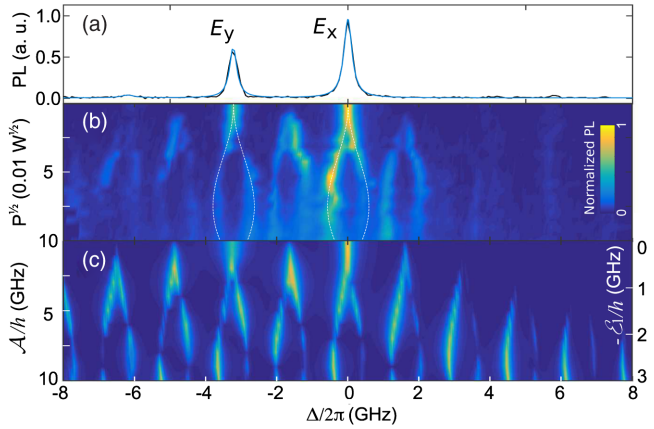

FIG. 3. (a) PLE scan of NV2, which has an $\{|E_x\rangle, |E_y\rangle\}$ state splitting of 3.2 GHz. (b) Experimental data from phonon-dressed state PLE. The mechanical driving frequency, $\omega_m/2\pi = 1.6$ GHz, matches half of the $\{|E_x\rangle, |E_y\rangle\}$ splitting. The dressed orbital states exhibit gigahertz-scale phonon Rabi splitting, which is well described by the $n = 1$ term in Eq. (4), $\mathcal{E}_1 \sin 2\theta J_1\{2[\mathcal{E}_1/(\hbar\omega_m)]\cos 2\theta\}$, which corresponds to a 2-phonon Rabi splitting (white dashed lines). (c) Reconstruction of experimental data with a quantum master equation simulation.

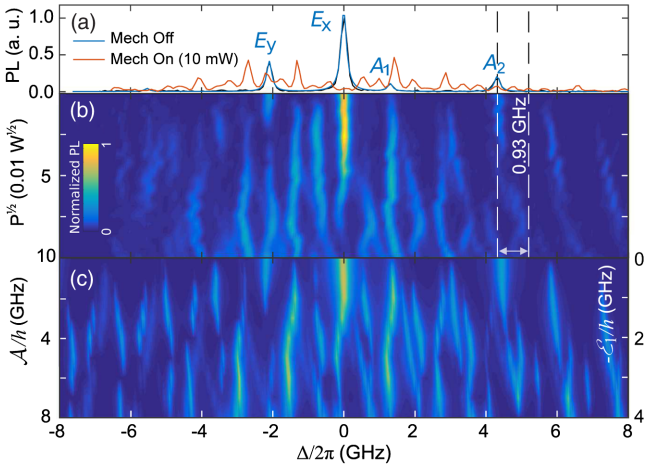

FIG. 4. (a) PLE scan of NV3 with $\{|E_x\rangle, |E_y\rangle\}$ state splitting of 2.1 GHz, taken with continuous wave 2.877 GHz magnetic microwave driving to the antenna. (b) Experimental data from phonon-dressed state PLE measurement of NV3 with $\omega_m/2\pi = 1.3844$ GHz. A Rabi splitting of 0.93 GHz in the $|A_2\rangle$ state is observed with 10 mW mechanical driving. (c) Reconstruction of experimental data using a quantum master equation simulation.

experiment. The simulations [Figs. 2(c), 3(c)] show excellent agreement to the measured spectra. For the case of NV2 with resonant-phonon driving, the gigahertz orbital Rabi splitting [Fig. 3(b)] implies that, after laser excitation to one of the orbital states, coherent Rabi oscillations between the two NV-center orbital states will occur on the timescale of a nanosecond (see Supplemental Material [29]), which is an order of magnitude smaller than the intrinsic excited state life time of NV centers [41].

Next, we probe electron-phonon coupling in the full six-level NV-center excited states on a third NV center (NV3) with a static strain splitting of 2.1 GHz. To spectroscopically access the orbital states with $m_s \neq 0$ character, we drive a continuous wave, 2.877 GHz current into the microwave antenna, which prepares NV3 in a mixed spin state prior to resonant laser excitation. This enables access to all excited-state optical transitions, i.e., $|^3A_2, |m_s| = 1\rangle \rightarrow |A_1\rangle$, $|^3A_2, |m_s| = 1\rangle \rightarrow |A_2\rangle$, $|^3A_2, |m_s| = 1\rangle \rightarrow |E_1\rangle$, and $|^3A_2, |m_s| = 1\rangle \rightarrow |E_2\rangle$ can all be excited, in addition to the ones studied above. A single PLE scan with magnetic microwave driving is shown in Fig. 4(a). The $|A_1\rangle$ and $|A_2\rangle$ orbital states are revealed on the right of E-state peaks, and $|E_{1,2}\rangle$ are out of the scanning range. The small peak on the left of Fig. 4(a) is from a non-spin-conserving transition between $|^3A_2, m_s = 0\rangle$ and the $|E_{1,2}\rangle$ states. The corresponding phonon-dressed state spectra ($\omega_m/2\pi = 1.3844$ GHz) is shown in Fig. 4(b). Here, $|A_1\rangle$ and $|A_2\rangle$ experience comparable modulation with $|E_x\rangle$ and $|E_y\rangle$ in response to a coherent phonon driving. Apart from the emergence of sideband transitions, 10 mW mechanical driving produces a phonon Rabi splitting of 0.93 GHz as a result of E_1 modulation induced mixing between $|A_1\rangle(|A_2\rangle)$ and $|E_1\rangle(|E_2\rangle)$ states [marked by the white arrow in Fig. 4(b)]. A resonant phonon field can thus drive orbital transitions between the $m_s \neq 0$ orbital levels in a similar way as $m_s = 0$ orbital levels, i.e., $|A_1\rangle \leftrightarrow |E_1\rangle$, $|A_2\rangle \leftrightarrow |E_2\rangle$. The dressed state spectra generally agree with our eight-level master equation simulation [29] results in Fig. 4(c). We attribute the mismatch in the simulated intensity of E_y sidebands to the intersystem crossing process through the singlet states [42].

We can evaluate the strength of A_1 and E_1 modulation generated by the HBAR device for each of the three NV centers by comparing the data and the simulation results. We find $\mathcal{E}_1/\mathcal{A} \sim -0.4(1)$ for all three NV centers. At modest mechanical driving power (10 mW), we observe phonon coupling up to $\mathcal{A}/h \simeq 13$ GHz. Using the previously measured coupling factor, 465 Hz/Pa [18,22,43], we estimate that the stress amplitude produced by the resonator is around 30 MPa, corresponding to a lattice strain of 7×10^{-6}, which is consistent with our previous work [12], and it is comparable to the strain generated in an oscillating cantilever system [22]. As such, dressed state spectroscopy provides a quantitative approach for ac strain characterization within a resonator (see Supplemental Material [29]).

Phonon-driven orbital transitions also provide a powerful method to control a NV-center orbital quantum state dynamically, for example, resonant Rabi driving between $|E_x\rangle$ and $|E_y\rangle$. Because electric fields and strains shift NV-center optical transitions in similar ways [44,45], a potential application of orbital Rabi driving is continuous dynamical decoupling (CDD) [46] of orbital states. Orbital CDD would operate in an analogous fashion to CDD of

spin states [14,47–50]: when driving an orbital transition on resonance, the dressed orbital eigenstates have $d\omega/d\epsilon_\perp = 0$, where ω is the optical transition frequency, and $\epsilon_\perp$ is the electric field strength transverse with respect to the NV axis. This would eliminate the NV center's sensitivity to the transverse components of the uncontrolled, environmental electric field fluctuations originating from, for example, charge repumping or surface charge fluctuations. This will make the optical transitions more robust to spectral diffusion and reduce inhomogeneous line broadening [51]. Therefore, coherent phonon-driven orbital control is an untapped resource for improving the optical properties of NV centers in support of quantum optical control [9–11], spin-photon entanglement [52,53], coupling to optical cavities [54], and other applications of resonant optical coupling.

In summary, we have experimentally examined the resonant optical transitions of a NV center subject to a coherent phonon drive. In the phonon-dressed orbital states, we observe a strong orbital-phonon interaction that gives rise to multiple Raman sidebands and a large phonon-induced Rabi splitting of the orbital states, which are due to A_1- and E_1-type phonon modulation, respectively. Finally, we show that resonant mechanical driving leads to multiphonon transitions between orbital states and discuss a potential application for orbital state decoherence protection.

We thank Kenneth W. Lee and Marcus W. Doherty for helpful discussions. Research support was provided by the Office of Naval Research (Grants No. N000141410812 and No. N000141712290). Device fabrication was performed in part at the Cornell NanoScale Science and Technology Facility, a member of the National Nanotechnology Coordinated Infrastructure, which is supported by the National Science Foundation (Grant No. ECCS-15420819), and at the Cornell Center for Materials Research Shared Facilities which are supported through the NSF MRSEC program (Grant No. DMR-1719875).

*gdf9@cornell.edu

[1] B. Hensen, H. Bernien, A. E. Drau, A. Reiserer, N. Kalb, M. S. Blok, J. Ruitenberg, R. F. L. Vermeulen, R. N. Schouten, C. Abelln, W. Amaya, V. Pruneri, M. W. Mitchell, M. Markham, D. J. Twitchen, D. Elkouss, S. Wehner, T. H. Taminiau, and R. Hanson, Nature (London) **526**, 682 (2015).

[2] J. R. Maze, P. L. Stanwix, J. S. Hodges, S. Hong, J. M. Taylor, P. Cappellaro, L. Jiang, M. V. Gurudev Dutt, E. Togan, A. S. Zibrov, A. Yacoby, R. L. Walsworth, and M. D. Lukin, Nature (London) **455**, 644 (2008).

[3] M. S. J. Barson, P. Peddibhotla, P. Ovartchaiyapong, K. Ganesan, R. L. Taylor, M. Gebert, Z. Mielens, B. Koslowski, D. A. Simpson, L. P. McGuinness, J. McCallum, S. Prawer, S. Onoda, T. Ohshima, A. C. Bleszynski Jayich, F. Jelezko, N. B. Manson, and M. W. Doherty, Nano Lett. **17**, 1496 (2017).

[4] F. Dolde, H. Fedder, M. W. Doherty, T. Nbauer, F. Rempp, G. Balasubramanian, T. Wolf, F. Reinhard, L. C. L. Hollenberg, F. Jelezko, and J. Wrachtrup, Nat. Phys. **7**, 459 (2011).

[5] L. Childress and R. Hanson, MRS Bull. **38**, 134 (2013).

[6] E. van Oort, N. B. Manson, and M. Glasbeek, J. Phys. C **21**, 4385 (1988).

[7] F. Jelezko, T. Gaebel, I. Popa, A. Gruber, and J. Wrachtrup, Phys. Rev. Lett. **92**, 076401 (2004).

[8] G. D. Fuchs, V. V. Dobrovitski, R. Hanson, A. Batra, C. D. Weis, T. Schenkel, and D. D. Awschalom, Phys. Rev. Lett. **101**, 117601 (2008).

[9] D. A. Golter and H. Wang, Phys. Rev. Lett. **112**, 116403 (2014).

[10] Y. Chu, M. Markham, D. J. Twitchen, and M. D. Lukin, Phys. Rev. A **91**, 021801(R) (2015).

[11] L. C. Bassett, F. J. Heremans, D. J. Christle, C. G. Yale, G. Burkard, B. B. Buckley, and D. D. Awschalom, Science **345**, 1333 (2014).

[12] E. R. MacQuarrie, T. A. Gosavi, N. R. Jungwirth, S. A. Bhave, and G. D. Fuchs, Phys. Rev. Lett. **111**, 227602 (2013).

[13] E. R. MacQuarrie, T. A. Gosavi, A. M. Moehle, N. R. Jungwirth, S. A. Bhave, and G. D. Fuchs, Optica **2**, 233 (2015).

[14] E. R. MacQuarrie, T. A. Gosavi, S. A. Bhave, and G. D. Fuchs, Phys. Rev. B **92**, 224419 (2015).

[15] E. R. MacQuarrie, M. Otten, S. K. Gray, and G. D. Fuchs, Nat. Commun. **8**, 14358 (2017).

[16] P. Ovartchaiyapong, K. W. Lee, B. A. Myers, and A. C. B. Jayich, Nat. Commun. **5**, 4429 (2014).

[17] J. Teissier, A. Barfuss, P. Appel, E. Neu, and P. Maletinsky, Phys. Rev. Lett. **113**, 020503 (2014).

[18] G. Davies and M. F. Hamer, Proc. R. Soc. A **348**, 285 (1976).

[19] A. Batalov, V. Jacques, F. Kaiser, P. Siyushev, P. Neumann, L. J. Rogers, R. L. McMurtrie, N. B. Manson, F. Jelezko, and J. Wrachtrup, Phys. Rev. Lett. **102**, 195506 (2009).

[20] K. V. Kepesidis, S. D. Bennett, S. Portolan, M. D. Lukin, and P. Rabl, Phys. Rev. B **88**, 064105 (2013).

[21] L. Giannelli, R. Betzholz, L. Kreiner, M. Bienert, and Giovanna Morigi, Phys. Rev. A **94**, 053835 (2016).

[22] K. W. Lee, D. Lee, P. Ovartchaiyapong, J. Minguzzi, J. R. Maze, and A. C. Bleszynski Jayich, Phys. Rev. Applied **6**, 034005 (2016).

[23] D. A. Golter, T. Oo, M. Amezcua, K. A. Stewart, and H. Wang, Phys. Rev. Lett. **116**, 143602 (2016).

[24] D. A. Golter, T. Oo, M. Amezcua, I. Lekavicius, K. A. Stewart, and H. Wang, Phys. Rev. X **6**, 041060 (2016).

[25] H. A. Jahn and E. Teller, Proc. R. Soc. A **161**, 220 (1937).

[26] A. E. Hughes and W. A. Runciman, Proc. Phys. Soc. London **90**, 827 (1967).

[27] M. Dresselhaus, *Applications of Group Theory to the Physics of Solids* (MIT, Cambridge, MA, 2002), Chapter 3.

[28] M. Lannoo and J. Bourgoin, *Point Defects in Semiconductors: I. Theoretical Aspects* (Springer, Berlin, 1981).

[29] See Supplemental Material at http://link.aps.org/supplemental/10.1103/PhysRevLett.120.167401 for details.

[30] T. Ishikawa, K. C. Fu, C. Santori, V. M. Acosta, R. G. Beausoleil, H. Watanabe, S. Shikata, and K. M. Itoh, Nano Lett. **12**, 2083 (2012).
[31] T. G. Thomas and S. C. Sekhar, *Communication Theory* (Tata-McGraw Hill, New York, 2005).
[32] M. Metcalfe, S. M. Carr, A. Muller, G. S. Solomon, and J. Lawall, Phys. Rev. Lett. **105**, 037401 (2010).
[33] M. Tanasittikosol and R. M. Potvliege, arXiv:1206.5951.
[34] D. Leibfried, R. Blatt, C. Monroe, and D. Wineland, Rev. Mod. Phys. **75**, 281 (2003).
[35] W. D. Oliver, Y. Yu, J. C. Lee, K. K. Berggren, L. S. Levitov, and T. P. Orlando, Science, **310**, 1653 (2005).
[36] S. K. Son, S. Han, and S.-I. Chu, Phys. Rev. A **79**, 032301 (2009).
[37] H. J. Metcalf and P. van der Straten, *Laser Cooling and Trapping* (Springer, New York, 2002).
[38] R. Silbey and R. A. Harris, J. Chem. Phys. **80**, 2615 (1984).
[39] S. Ashhab, J. R. Johansson, A. M. Zagoskin, and F. Nori, Phys. Rev. A **75**, 063414 (2007).
[40] P. Rabl, Phys. Rev. B **82**, 165320 (2010).
[41] A. Batalov, C. Zierl, T. Gaebel, P. Neumann, I.-Y. Chan, G. Balasubramanian, P. R. Hemmer, F. Jelezko, and J. Wrachtrup, Phys. Rev. Lett. **100**, 077401 (2008).
[42] M. L. Goldman, M. W. Doherty, A. Sipahigil, N. Y. Yao, S. D. Bennett, N. B. Manson, A. Kubanek, and M. D. Lukin, Phys. Rev. B **91**, 165201 (2017).
[43] M. W. Doherty, V. V. Struzhkin, D. A. Simpson, L. P. McGuinness, Y. Meng, A. Stacey, T. J. Karle, R. J. Hemley, N. B. Manson, L. C. L. Hollenberg, and S. Prawer, Phys. Rev. Lett. **112**, 047601 (2014).
[44] J. R. Maze, A. Gali, E Togan, Y. Chu, A. Trifonov, E. Kaxiras, and M. D. Lukin, New J. Phys. **13**, 025025 (2011).
[45] M. Doherty, N. B. Manson, P. Delaney, and L. C. L. Hollenberg, New J. Phys. **13**, 025019 (2011).
[46] F. F. Fanchini, J. E. M. Hornos, and R. d. J. Napolitano, Phys. Rev. A **75**, 022329 (2007).
[47] P. Rabl, P. Cappellaro, M. V. Gurudev Dutt, L. Jiang, J. R. Maze, and M. D. Lukin, Phys. Rev. B **79**, 041302(R) (2009).
[48] X. Xu, Z. Wang, C. Duan, P. Huang, P. Wang, Y. Wang, N. Xu, X. Kong, F. Shi, X. Rong, and J. Du, Phys. Rev. Lett. **109**, 070502 (2012).
[49] D. A. Golter, T. K. Baldwin, and H. Wang, Phys. Rev. Lett. **113**, 237601 (2014).
[50] A. Barfuss, J. Teissier, E. Neu, A. Nunnenkamp, and P. Maletinsky, Nat. Phys. **11**, 820 (2015).
[51] K.-M. C. Fu, C. Santori, P. E. Barclay, L. J. Rogers, N. B. Manson, and R. G. Beausoleil, Phys. Rev. Lett. **103**, 256404 (2009).
[52] E. Togan, Y. Chu, A. S. Trifonov, L. Jiang, J. Maze, L. Childress, M. V. G. Dutt, A. S. Srensen, P. R. Hemmer, A. S. Zibrov, and M. D. Lukin, Nature (London) **466**, 730 (2010).
[53] H. Bernien, B. Hensen, W. Pfaff, G. Koolstra, M. S. Blok, L. Robledo, T. H. Taminiau, M. Markham, D. J. Twitchen, L. Childress, and R. Hanson, Nature (London) **497**, 86 (2013).
[54] R. Albrecht, A. Bommer, C. Deutsch, J. Reichel, and C. Becher, Phys. Rev. Lett. **110**, 243602 (2013).